

Deep Learning-driven Community Resilience Rating based on Intertwined Socio-Technical Systems Features

Kai Yin¹, Ali Mostafavi^{1*}

¹ Urban Resilience.AI Lab, Zachry Department of Civil and Environmental Engineering, Texas A&M University, College Station, United States

* Corresponding author: Ali Mostafavi, amostafavi@civil.tamu.edu

Abstract

Community resilience is a complex and multi-faceted phenomenon that emerges from complex and nonlinear interactions among different socio-technical systems and their resilience properties. However, present studies on community resilience focus primarily on vulnerability assessment and utilize index-based approaches, with limited ability to capture heterogeneous features within community socio-technical systems and their nonlinear interactions in shaping robustness, redundancy, and resourcefulness components of resilience. To address this gap, this paper presents an integrated three-layer deep learning model for community resilience rating (called *Resili-Net*). Twelve measurable resilience features are specified and computed within community socio-technical systems (i.e., facilities, infrastructures, and society) related to three resilience components of robustness, redundancy, and resourcefulness. Using publicly accessible data from multiple metropolitan statistical areas in the United States, *Resili-Net* characterizes the resilience levels of spatial areas into five distinct levels. The interpretability of the model outcomes enables feature analysis for specifying the determinants of resilience in areas within each resilience level, allowing for the identification of specific resilience enhancement strategies. Changes in community resilience profiles under urban development patterns are further examined by changing the value of related socio-technical systems features. Also, combined resilience-risk levels in each community are analyzed, and several communities are found to suffer from high risk and low resilience, which calls for special attention to resilience enhancement. Departing from the dominantly vulnerability-focused assessments, *Resili-Net* enables characterizing community resilience as an emergent property arising from nonlinear interactions among heterogeneous community features related to their socio-technical systems. Accordingly, the outcomes provide novel perspectives for community resilience assessment by harnessing machine intelligence and heterogeneous urban big data.

Keywords: Urban resilience rating, Socio-technical systems, Spatial distribution, Combined resilience-risk assessment

Introduction

Natural hazards pose a significant threat to cities and communities across the globe¹. Trends of population growth and urbanization continue in the future, more and more population and assets will be exposed to hazard threats¹⁻³. Hence, assessing the risk and resilience of cities and communities is of paramount importance for developing and implementing plans and policies to effectively cope with these hazards. Of particular importance are assessments that characterize the risk and resilience profile of communities and cities to reveal spatial variations for informing plans and actions. Recognizing this, multiple studies⁴⁻⁶ have proposed vulnerability assessment methods and rating indices for mapping the vulnerability profiles of cities and communities. However, vulnerability assessment methods fail to capture important community features that shape the three elements of resilience related to robustness, redundancy, and resourcefulness across the community socio-technical systems.

Also, previous research on community resilience focused mostly on a particular sub-system. Frequently studied are transportation systems⁷⁻¹⁰, power systems^{11,12}, communication systems¹³, and social systems¹⁴. While these studies provide insights about the resilience of individual systems, they fail to provide comprehensive resilience ratings across different areas of a community. In fact, cities are complex systems with features related to different socio-technical systems, such as the built environment, society, and infrastructures that nonlinearly and dynamically interact with each other, giving rise to community resilience^{1,15}, among other urban phenomena. Hence, methods used for determining the resilience profile of cities and communities should be capable of capturing the complex and nonlinear interactions among heterogeneous features related to community socio-technical systems to provide a proper characterization of the underlying complexity.

In another stream of research and in efforts to characterize the resilience profiles of cities and communities, researchers Huang et al.¹⁶ and Parizi et al.¹⁷ proposed methods that select resilience assessment indicators, then assign weights to each resilience indicator, and finally aggregate multiple indicators into a single synthetic score to assess resilience. In this indicator-based assessment approach. Determining the weights assigned to each indicator is mostly expert-based or equal weight assignment, which is rather subjective¹⁸. Another major restriction of these methods is their limited ability to capture the nonlinear and complex interactions among resilience features associated with different elements of socio-technical systems. In fact, community resilience emerges from the complex and nonlinear interactions among heterogeneous resilience-related features. Hence, indicator-based methods are rather simplistic in capturing the emergent nature of community resilience shaped by complex and nonlinear interactions among various community features.

Recognizing these important gaps related to a comprehensive and data-driven characterization of resilience profiles of communities and cities, we propose an integrated three-layer unsupervised deep learning model for community resilience rating (called *Resili-Net*) to characterize community resilience profiles in cities using urban big data and machine intelligence. *Resili-Net* is capable of capturing the complex and nonlinear interactions among multiple heterogeneous features related to the three resilience components of robustness, redundancy, and resourcefulness across different elements of community socio-technical systems: facilities, infrastructure, and society. We evaluate the *Resili-Net* model in four of the most populous metropolitan statistical areas in the United States: Los Angeles, Chicago, Dallas, and Houston. The model rates the resilience level of spatial grid cells based on their underlying features. Upon specification of the resilience levels of different areas within each MSA, we map the risk-resilience profile to identify high-risk and low-resilience areas as critical zones needing targeted risk reduction and resilience enhancement plans and actions.

The main novel aspects of this study are fivefold: (1) Specifying twelve measurable resilience features related to the three resilience components of robustness, redundancy, and resourcefulness across different community socio-technical systems components (i.e., facilities, infrastructures, and society). (2) Creating an integrated three-layer neural network model for community resilience rating capable of capturing the complex and nonlinear interactions among different resilience characteristics associated with intertwined sociotechnical systems features. (3) Uncovering five distinct community resilience levels within each MSA for resilience rating

and spatial assessment. (4) Unveiling the determinants of resilience levels across different areas based on interpretation of features distribution of each cluster. (5) Specifying the combined resilience-risk levels of areas for targeted resilience enhancements focusing on high-risk, low resilience communities; the combined resilience-risk analysis also unveils the consideration of optimum infrastructure development in order to balance risk and resilience levels. These contributions offer significant advancements, moving the interdisciplinary fields of community resilience and disasters closer to more data-driven, intelligent, and complexity-focused characterization of resilience in cities and communities.

Results

Three-layer unsupervised deep learning model for community resilience rating. An integrated three-layer deep learning model for community resilience rating, *Resili-Net* (Fig.1; see Methods for details), is based on multiple features related to the three components of resilience: robustness, redundancy, and resourcefulness using publicly available datasets. Table 1 summarizes the features used in the model. The description and computation of features, as well as the rationale for their selection, are explained in the Methods section.

In the first layer, node representation learning, the complex and nonlinear interactions of resilience-related features (**RF**, Table 1) among different urban sub-systems are encoded into latent representations. In the second layer, grid cells with similar resilience levels are clustered into the same group by implementing a deep clustering module on the learned node representation. In the third layer, feature importance is determined by utilizing clustering results as labels for classification algorithms and then interpreting cluster assignments modeled by the classifier. The community resilience level of each cluster is calculated by taking feature importance as weights.

Table 1 Features used to assess community resilience

Urban Sub-systems	Robustness	Redundancy	Resourcefulness
Facility	Building Age	Number of hospitals within 30-min. driving distance	Area of green space
Infrastructure-Transportation	Degree assortativity coefficient	Number of roads connected with grid cell	Road length
Infrastructure-Communication	Cell tower age	Number of cell towers	Internet speed
Society	Poverty rate	Social Connectedness	Education level

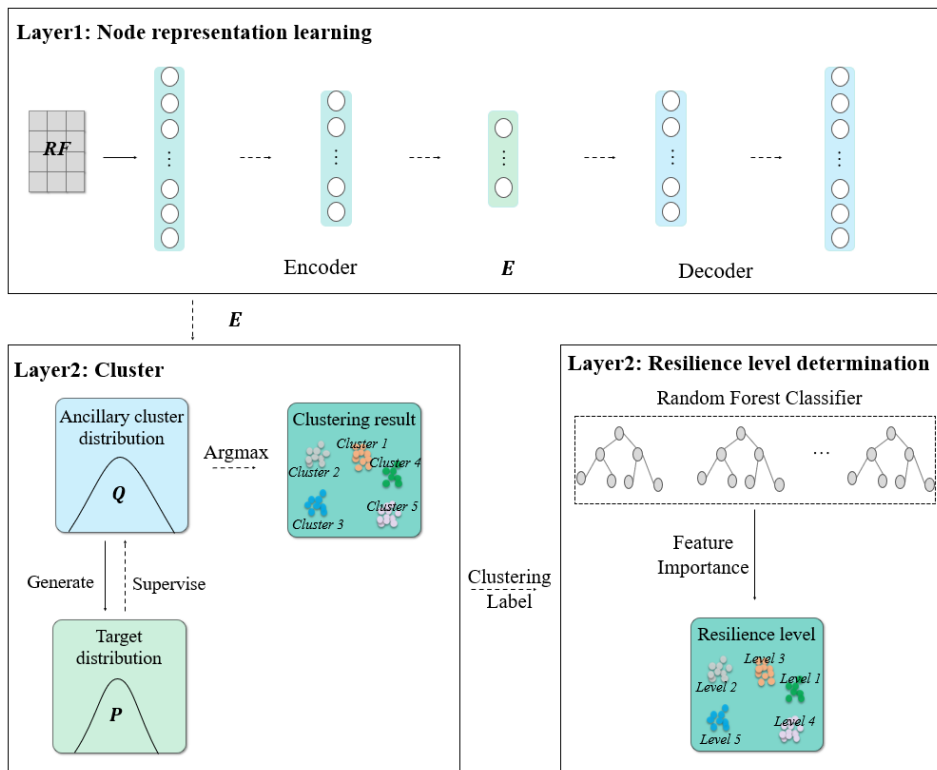


Fig. 1 | The overall framework of the proposed three-layer community resilience-rating model. Each MSA is divided into grid cells of equal size. Areas in each grid cell are assumed to have the same flood-risk level. The input of the model is resilience-related features matrix (RF) which includes three resilience characteristics of robustness, redundancy, and resourcefulness in three urban sub-systems of facilities, infrastructures, and societies (Table 1; See the Methods for details about the construction of

RF). The model outputs the resilience level of each grid cell. *E* is the encoded representation of *RF*.

Revealing five resilience levels within each MSA based on interactions among community resilience-related features. *Resili-Net* yields five distinct, city-specific community resilience levels, with level 5 being the highest resilience, while level 1 being the lowest resilience level (Fig. 2). These outputs unveil the spatial profile of community resilience across different areas of cities in an interpretable way. Each resilience level has distinct feature values related to the extent of robustness, redundancy, and resourcefulness of the three urban sub-systems (Fig. 3). For example, the highest resilience-level areas in Greater Houston are found to have the lowest building age, cell tower age, and poverty rate as well as the largest available number of healthcare centers within 30 minutes' driving distance, the largest number connected to the community, the largest available number of cell towers; and the largest road length, the fastest internet speed, and the highest education level. All of these features indicate that these communities have the greatest levels of robustness, redundancy, and resourcefulness, giving them the highest capacity to prepare for, absorb, recover from, and adapt to disturbances caused by hazards.

Overlapping the boundaries of each MSA's core city and the resilience map shows that communities with the greatest resilience usually lie in or near the core city of each MSA. Comparisons between characteristics of feature distribution in core cities and other areas in each MSA (Fig.4) reveal that facilities and infrastructures are usually newly updated and centralized in the core city of each MSA. This urban forms and structures of centralized distribution of updated facilities and infrastructures bring the city center with larger redundancy, resourcefulness and robustness, which yields better resilience in the core city.

Concentrations of community resilience are found to be spatially distributed instead of randomly distributed and dispersed. Global Moran's I index is calculated by taking contiguous network (grid cell sharing a boundary or a vertex are defined as a neighbor) as spatial-weight matrix. The large positive values of global Moran's I with the small enough *p*-values (Table 2) quantitatively illustrate that contiguous communities tend to have similar community resilience levels. This spatial autocorrelation of areas with similar community resilience levels suggests that community resilience enhancement measures in one area would have possible spillover effects and would also impact the community resilience level of neighboring areas. Conversely, development patterns in one area could reduce resilience level in the neighboring areas.

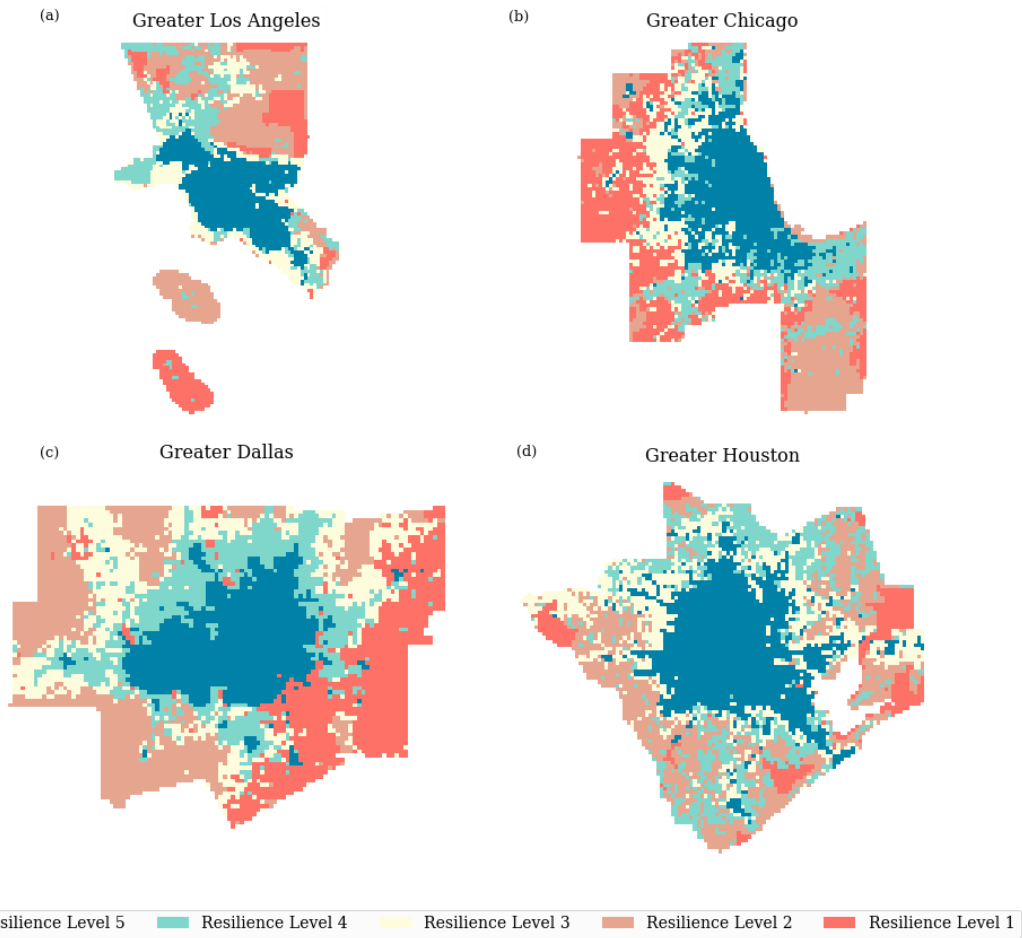


Fig. 2 | Geographical distribution of flood-risk level in four MSAs. Geographical distribution of flood-risk levels in (a) Greater Los Angeles, (b) Greater Chicago, (c) Greater Dallas, (d) Greater Houston.

Table 2 Results of Global Moran's I index in four MSAs

<i>MSAs</i>	<i>Greater Los Angeles</i>	<i>Greater Chicago</i>	<i>Greater Dallas</i>	<i>Greater Houston</i>
Moran's I value	0.851***	0.768***	0.821***	0.698***

*** significant at 0.01 level

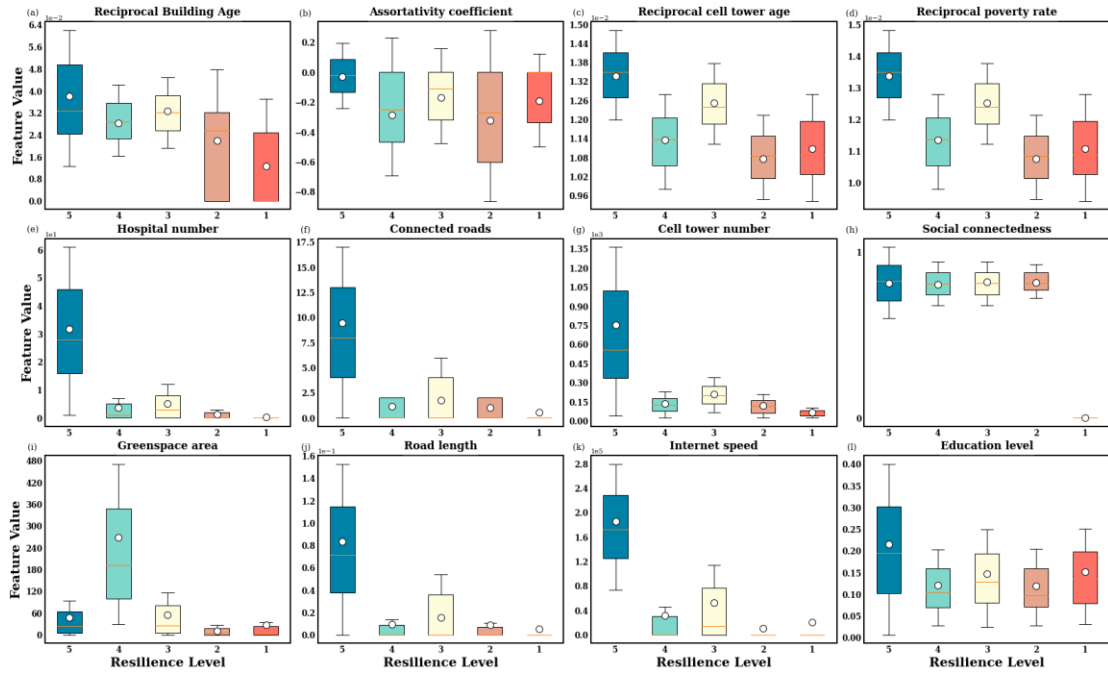


Fig.3 | Characteristics of clusters in Greater Houston. Community resilience comprises the characteristics of (a) reciprocal building age, (b) assortativity coefficient, (c) reciprocal cell tower age, (d) the reciprocal rate of poverty, (e) the number of healthcare centers within 30 minutes' driving distance, (f) the number roads connected to the grid cell, (g) the number of cell towers, (h) social connectedness, (I) the area of greenspace, (j) road length, (k) internet speed, and (l) education level. (The other three MSAs are shown in Supplementary Figures 13.)

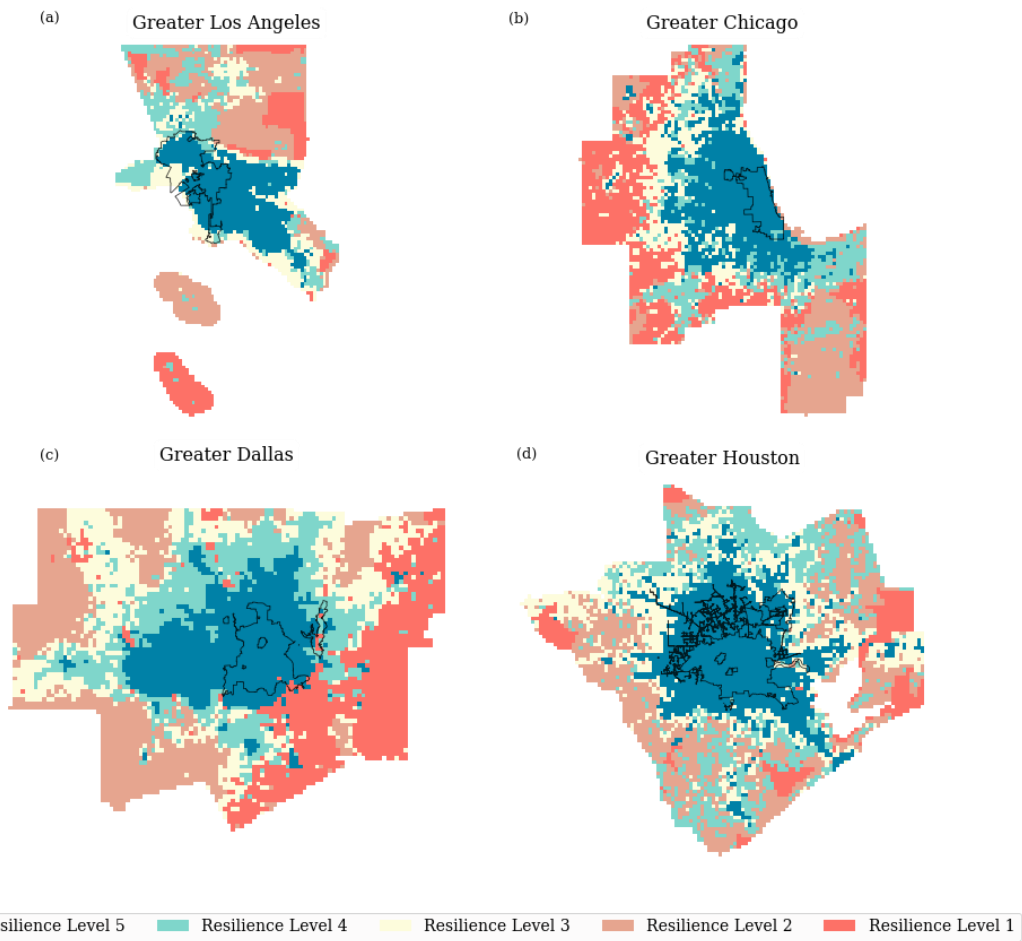


Fig 4 | Overlapping the boundary of each MSA’s core city and the community resilience map. Core cities for these four MSAs are (a) Los Angeles, (b) Chicago, (c) Dallas, and (d) Houston.

Changes in resilience level under urban development. Urban development and growth patterns reshape the spatial profile of community resilience. *Resili-Net* could be implemented to generate a community's resilience level for different urban development scenarios by changing the input value of community socio-technical features. For example, for a hypothetical scenario that, for communities with the poorest resilience level, both the number of hospitals within 30 minutes driving distance and the road length will increase twenty percent. Changes of these resilience-related features represent urban development and the *Resili-Net* is re-trained to adapt to these changes.

MSAs show considerable differences in the change of community resilience levels when urban features change (Fig. 5). In Greater Los Angeles, some communities would witness a boost in resilience levels by a single tier. This indicates that strategies focusing on healthcare accessibility and transportation infrastructure may be particularly effective in these areas. In contrast, the Greater Chicago area presents a more complex picture. While some communities would see an improvement in resilience, others would experience a decline. This suggests that a one-size-fits-all approach would not be applicable, necessitating more nuanced, localized strategies. Moreover, it implies that factors other than hospital accessibility and road length, such as social cohesion, could be at play and require separate interventions. Within the MSAs for Greater Dallas and Houston, most communities' resilience levels remain unchanged under further urban development, but communities with improved or deteriorated resilience are dispersed across a city. This result suggests that mere infrastructure development, such as hospitals and roads, might not be sufficient to improve resilience universally in all areas of a city. Rather, attention should be given to enhancing social infrastructure, such as green spaces, especially in areas already abundant in physical infrastructure.

This heterogeneous community response is due to the intricate interactions among components of socio-technical systems within urban environments, such as social, facility, and infrastructural systems. This complexity underscores the necessity of capturing these interactions to develop targeted resilience enhancement strategies. For instance, communities with already robust and redundant road networks and hospital accessibility may not benefit substantially from further improvements in these domains. Instead, the strategic focus should shift towards improving social infrastructure, such as increasing green spaces, which not only elevates community well-being but also contributes to resilience in other ways, such as enhancing social cohesion. These strategies could be informed by a deep understanding of the multifaceted interactions among community socio-technical systems which has already been captured by the *Resili-Net* model.

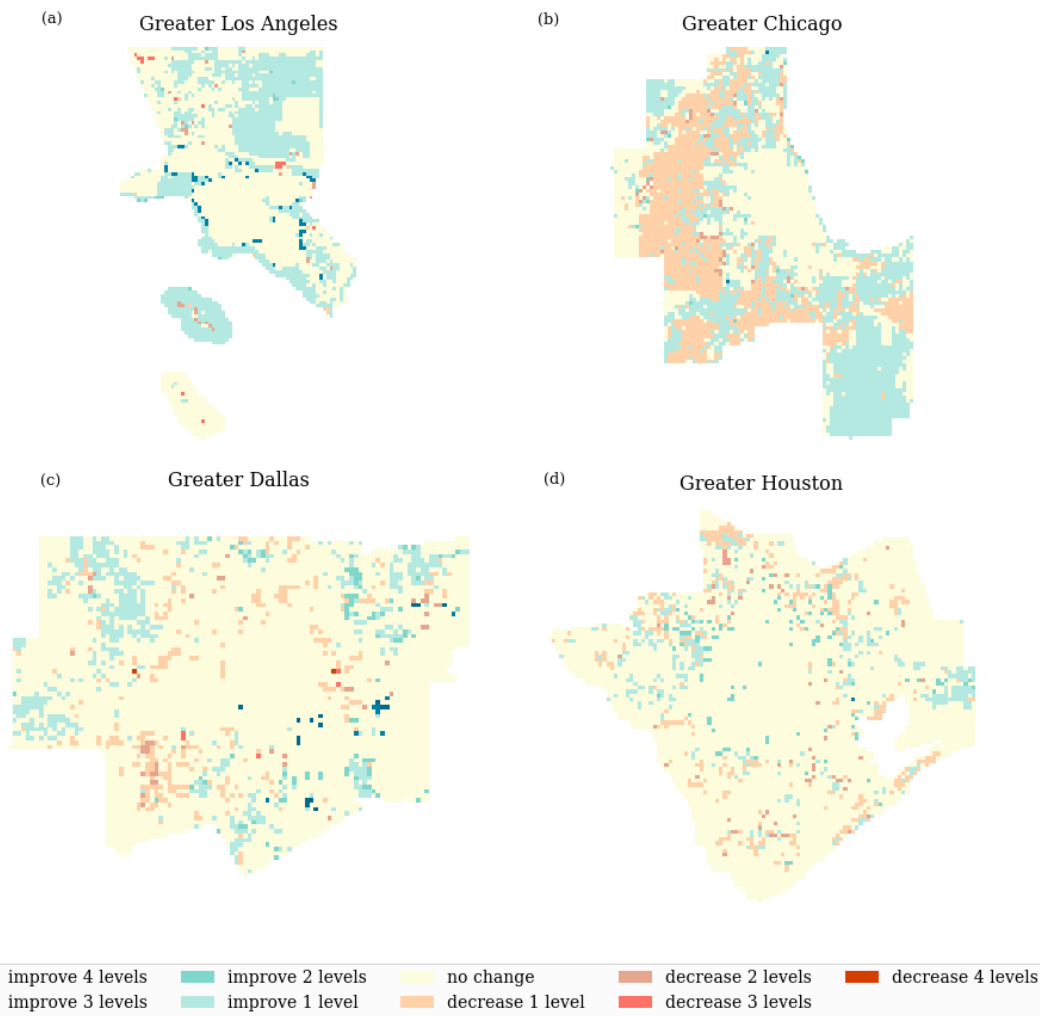


Fig.5 | Spatial distribution of community resilience level changes under urban development. Each community’s resilience level after urban development is compared with the previous resilience level. Urban development is modeled by the changes of the input features value. The spatial distribution of community resilience level after urban development is shown in Fig. S7 in the Supplementary Material.

Combined resilience-risk levels. Community resilience levels capture the ability of a community to prepare for, absorb, recover from, and adapt to disturbances¹⁹, while the risk level measures the extent of hazard exposure and vulnerability in the community²⁰. Hence, a combined resilience-risk assessment would provide a more comprehensive understanding of the extent of risks in a community and the ability of the community to cope with the risks. In this step, an analysis of the combined resilience and risk levels across different areas in four cities informs risk mitigation and resilience enhancement plans and actions. The flood risk level of areas is computed using the *FloodRisk-Net* model developed by Yin and Mostafavi²⁰. *FloodRisk-Net* captures features of hazards, exposure, and social and physical vulnerability in specifying flood risk levels of spatial areas. While the combined resilience-risk assessment in this step focuses on flood risk, one can replace this flood risk with risk levels for other hazards for a similar assessment.

The analysis reveals the ability of areas suffering from high flood risk level and low-resilience ability to deal with potential impacts caused by disasters (Fig. 6). The main determinants that shape high risk and low resilience in these areas are lack of infrastructure robustness and redundancy as well as greater social vulnerability and low resourcefulness of the populations (Fig. 5). Features of robustness, redundancy, and resourcefulness in these areas are all worse than other areas. The high-risk and low-resilience areas are where socially vulnerable populations reside with greater rates of unemployment, disability, elderly and children. All of these features make these communities susceptible to disasters with limited ability to prepare for, absorb, recover from, and adapt to disturbances. These are areas where infrastructure investments can be optimized to shift resources to other high-risk, low-resilience areas. This requires a nuanced approach to ensure that reducing the allocation of resources does not unintentionally decrease the resilience level.

Analyses of characteristics of areas in high-high and low-low categories (Figs. S8 and S9) show that the effects of facilities and infrastructures on community resilience and flood risk are twofold. The infrastructure and large available number of facilities increases the resourcefulness and redundancy of these communities, which is beneficial to the communities' resilience. These extensive physical infrastructure developments would also increase physical vulnerability which increases the flood risk level of the community. Another interesting observation is that in the low-low areas, the low level of resilience may not be a pressing concern due to the relatively low flood-hazard exposure. Nevertheless, while the focus on these areas may not be urgent, it should not be entirely ignored. Infrastructure in these areas should be gradually improved to ensure basic robustness and redundancy, preparing for unforeseen flood risks that may manifest due to climate change or other variables. For high-high areas, the existence of robust infrastructure, redundant systems, and high resourcefulness contribute to their ability to cope with high risks effectively. It could be tempting to allocate fewer resources to these areas because they already possess high resilience. However, strategies based on low-impact development and risk reduction measures are needed to reduce the risk of these areas. The focus in these areas should be on implementing strategies such as green infrastructure to enhance risk and resilience simultaneously rather than a further physical infrastructure development that would increase risk without changing resilience considerably.

To further enhance resilience, integrated urban design strategies should be specifically designed for the different types of areas. In high-low areas, retrofitting existing infrastructure to maintain robustness could be a viable strategy. High-low areas could serve as places for establishment of community centers (e.g., shelters) to enhance the overall community. The high social vulnerability in low-high areas with a large percentage in poverty contributes to low robustness and resourcefulness in these areas. To enhance their robustness, infrastructure development strategies should focus on risk reduction and resilience improvement simultaneously. By focusing on these aspects, communities can develop targeted and effective resilience enhancement and risk reduction strategies that account for co-benefits and trade-offs among socio-technical features shaping the varying degrees of flood risk and resilience in different areas. This comprehensive approach ensures that efforts to enhance community resilience are equitable and effective in the long term.

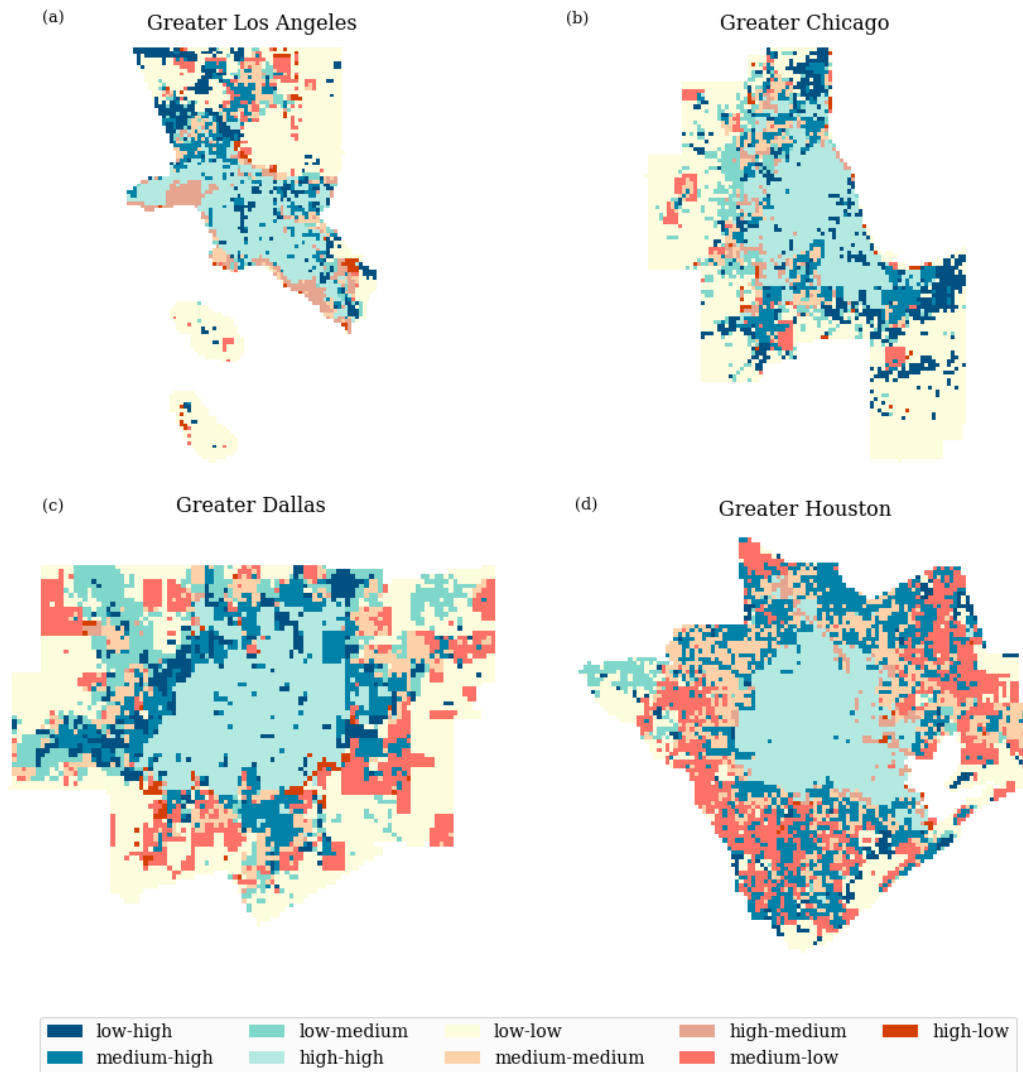


Fig. 6 | Spatial distribution of the comparison of community resilience and risk level. Both community resilience level and flood risk level are further divided into three types: low, medium, and high. For community resilience: levels 1 and 2 are considered as poor; level 3, medium; levels 4 and 5, good. For flood risk: levels 1 and 2 are considered low; levels 3 and 4, medium; and levels 5 and 6, high. Low-high represents low flood risk level and high community resilience level, the other eight annotations follow the same pattern; that is, the first item represents flood risk level, and the second one is the community resilience level.

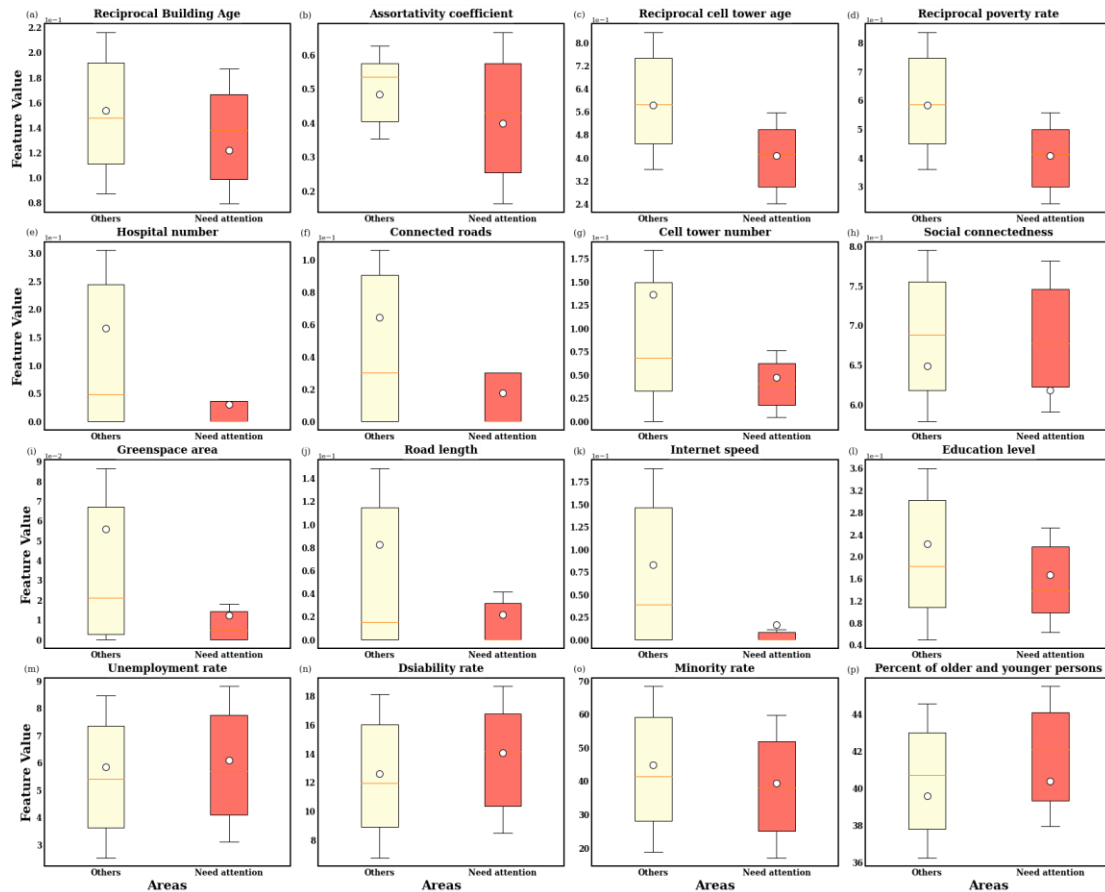


Fig.7 | Comparisons between characteristics of clusters in areas need special attention and other areas in Greater Houston. Areas needing special attention are characterized as high-poor, high-medium, and medium-poor in Fig. 6 due to their high-risk level and poor community resilience level. The last four of these sixteen features are selected to further evaluate the social vulnerability of communities following Yin and Mostafavi²⁰'s work. These four features are calculated using Centers for Disease Control/Agency for Toxic Substances and Disease Registry Social Vulnerability Index dataset²¹. Percent of older and younger persons is the rate of persons are aged 17 and younger and persons aged 65 and older. (The other three MSAs are shown in Supplementary Figures 4–6.)

Discussion

A novel deep learning model, *Resili-Net*, was developed in this study for examining the community resilience profile of cities based on their intertwined socio-technical systems features. *Resili-Net* contains three components: 1) node representation learning to encode complex and nonlinear interactions among twelve resilience-related features among three sub-urban systems; 2) resilience level cluster, clustering grid cells with similar resilience level into the same group; 3) resilience level determination, feature importance is integrated to determine the community resilience level of each cluster. *Resili-Net* specifies the twelve measurable resilience features related to the three resilience components (robustness, redundancy, and resourcefulness) across different socio-technical systems (i.e., facilities, infrastructures, and society). Using *Resili-Net*, city-specific community resilience profiles are obtained by disentangling complex interactions among these twelve resilience-related features.

The findings provide multiple important contributions to the community resilience assessments. First, departing from current research that merely focused on single components of community socio-technical systems, this study evaluates community resilience from a holistic perspective considering intertwined features related to different socio-technical systems shaping the three resilience components in communities. This integrated perspective could yield deeper, more nuanced insights into various socio-technical system features and their nonlinear interactions shaping community resilience profiles of cities. The methods presented in this study are generalizable across different cities and communities, as they allow for the development of resilience rating models based on publicly available datasets related to the socio-technical systems features.

Second, the findings reveal the spatial profile of resilience levels across different areas of cities. The spatial community resilience profiles are shaped by urban forms and structures, such as the centralized distribution of facility and infrastructure in city centers, yielding greater resilience levels. The spatial distribution of community resilience profiles provides important insights for current and future urban growth and infrastructure development strategies to account for the resilience levels of different areas and considers the ways in which future developments could enhance or exacerbate the resilience of different areas.

Third, we demonstrate heterogeneous responses to socio-technical system features changes across cities, which reveal that one-size-fits-all approaches would not be applicable to resilience enhancement across different cities, and underscores the requirements that resilience enhancement strategies be highly targeted and adapted to the specific characteristics and contexts of individual communities within each MSA. This data-driven method benefits policymakers by guiding them toward effective resilience enhancement strategies tailored to each MSA (and away from general solutions that may not be effective for all cities or neighborhoods).

Fourth, the combined resilience-risk assessment specifies high-risk, low-resilience areas within each MSA as critical areas needing special risk reduction and resilience enhancement plans and actions. The findings unveil the dual effects of developments in facilities and infrastructures: in areas with already high resilience levels, greater infrastructure development could increase risk without considerable enhancement in resilience. This finding supports the notion of optimum development in which the extent of infrastructure and facility developments should yield the greatest resilience level without compromising risk by increasing physical vulnerability. The high-high areas could benefit from alternative resilience enhancement strategies, such as low-impact development and social infrastructure development. The low-low areas may serve as areas for further infrastructure development to maintain economic growth and prosperity of cities. The high-low areas could play an important role in diffusion of resources to low-high areas in times of disasters. Infrastructure and facilities in high-low areas could serve populations in low-high areas during disasters impacts.

Accordingly, the model and findings provide particularly valuable insights to various academic disciplines and diverse stakeholder practitioners: (1) *Resili-Net* provides a novel method for urban scientists, designers and resilience officials to quantify, analyze, and monitor the resilience profile of cities and communities based on heterogeneous features related to various community socio-technical systems; (2) The specification of main features shaping the

resilience status of each spatial area provides data-driven insights for urban planners and infrastructure managers to devise resilience enhancement strategies for areas with low resilience levels. (3) Complementing the mainstream research focusing on community vulnerability and risk rating methods, *Resili-Net* and the resilience levels outputs provide public officials, city managers, and disaster researchers with new method and insights to evaluate risk and resilience profile of cities simultaneously to inform plans and projects; (4) The consideration of resilience as an emergent property of cities and communities and the capability of *Resili-Net* in capturing complex and nonlinear interactions among intertwined features of community socio-technical systems provide urban complexity researchers and geo-spatial scientists with fresh tool and insights to better capture and understand the complexity of community resilience extending beyond the rather simplistic index-based approaches.

Methods

Overview of resilience related feature matrix construction

Twelve resilience-related features pertinent to the three resilience components (robustness, redundancy, and resourcefulness) in urban sub-systems of facilities, infrastructure, and societies (shown in Table 1) are computed to construct the resilience feature matrix ($RF \in R^{m \times 16}$ being the number of grid cells in each MSA). These resilience-related features are at scales ranging from census-tract level to highly-detailed geographic coordinates. The study area is divided into 2 km \times 2 km grid cells respecting both the computation cost and the need for proper scale of analysis related to community resilience profiles. Community resilience-related features are aggregated at the grid-cell level. Each column in RF represents a resilience-related feature, and every row records resilience features for a grid cell.

Building age, which is calculated using National Structure Inventory (NSI)²² dataset, is used to measure the robustness of the facility. The number of hospitals within 30 minutes' driving distance measures the redundancy of a facility using SafeGraph point-of-interest (POI) data and OpenStreetMap road data (<https://www.openstreetmap.org/>). The greenspace area indicating potential areas for emergency shelters is adopted to measure resourcefulness of facility using National Land Cover Database (NLCD) (<https://www.usgs.gov/centers/eros/science/national-land-cover-database>). Two important infrastructures are considered: transportation and communication system. The degree assortativity coefficient, the number of roads connecting the grid cells, and road length are used to measure the robustness, redundancy, and resourcefulness of transportation system, using OpenStreetMap road data. Cell tower age and the available number of cell towers measure the robustness and redundancy of communication system using OpenCellID dataset (<https://opencellid.org/>). Internet speed measure the resourcefulness of communication system using Ookla's dataset (<https://www.ookla.com/ookla-for-good/open-data>). Poverty rate and education level measure the robustness and resourcefulness of society, respectively, using a US Census Bureau dataset (<https://data.census.gov/>). The social connectedness index measures the redundancy of society using Social Capital Atlas dataset (<https://socialcapital.org/>)²³. Data sources of community resilience assessment features are summarized in Table S1.

Selection of resilience characteristics and urban sub-systems

The community is the emergent property arising from complex interactions among several **urban sub-systems** such as facilities, population and infrastructures connecting them (e.g., transportation system, power system, communication network). Several **resilience characteristics** have been proposed by previous researchers to model resilience, ranging from the famous 4Rs (robustness, redundancy, resourcefulness, and rapidity)²⁴ to flexibility, efficiency, equality, and diversity^{14,16,25,26}. Three criteria are set to select suitable resilience features:

1. *Objectively measurable*. It refers to the ability to quantify or evaluate resilience based on data, rather than personal opinions, interpretations, or biases. Some resilience characteristics, such as resident's trust to the community, cannot be objectively measured by urban big data¹⁴.
2. *Directly measurable*. It refers to a characteristic or feature that can be observed and recorded without the need for further interpretation or inference. Some resilience characteristics are the result of other characteristics. For example, rapidity is the result of improvements in robustness, redundancy, and resourcefulness^{27,28}.
3. *Heterogeneous values*. There should be possible differences in the feature values among different grid cells, so that we can distinguish them. Some features may be the same within the city range due to the data scale. For example, the characteristics of resourcefulness is usually related to the adequacy of resources at the disposal of urban planners and decision makers to appropriately identify, prepare for, respond to, and recover from potential disruptions. Data for most of these resources (e.g., warning system, rescue resources, post-disaster recovery materials) is usually at the city- or state-scale. There are few differences between each spatial grid cell due to the data scale.

Measurement of robustness

Robustness denotes the level of performance that can be retained under perturbation²⁹. Building age measures the robustness of the facility. As summarized by Yin and Mostafavi²⁰, older buildings constructed are less advanced than the newly built ones considering their structure materials, construction practices, and building codes; thus older buildings tend to have a higher risk of structure damage under disruptive events^{30–32}. The National Structure Inventory (NSI) dataset which provides building age information in the census-tract level was adopted. Following Yin and Mostafavi²⁰'s work, the building age of each grid cell is calculated by the mean value of building age across all census tracts intersected with it as shown in Equation 1.

$$GC_BA_i = \frac{\sum_j CS_BA_j}{|BA_i|} \text{ for } j \text{ in } BA_i \quad (1)$$

where, GC_BA_i is the building age of grid cell i , CS_BA_j is the building age of census tract j , BA_i is the set of census tracts intersected with grid cell i , and $||$ is the number of elements in the set (the same hereafter).

Two key infrastructures are considered in community resilience assessment—transportation system and communication system—given data availability and their importance in urban systems^{33–36}. Assortativity coefficient is adopted to evaluate the robustness of the transportation systems. Assortativity coefficient, which measures the tendency for nodes in a network to connect to other nodes that are similar^{37,38}, is a particularly adequate robustness indicator used in network science literature³⁹. Simulation results of real-world road networks conducted by Dong et al⁴⁰ showed that node degree assortativity has a significant impact on road network robustness, and the correlation between node degree assortativity and road network robustness is positive. Dataset from OpenStreetMap is adopted by modeling road intersections as nodes and road segments as links in the graph. Following Yin et al¹⁰'s work, ten types of roads are considered in the model, and the graph is simplified by removing nodes whose degree is 2. This road network is constructed considering trade-offs between computation cost and real-world preservation. That is, include as many types of roads as possible to preserve real-world information and ensure the computation time is acceptable. This road network will also be used to calculate the redundancy and resourcefulness of the transportation system, and the travel distance between each grid cell, which is needed in calculating the redundancy and the resourcefulness of the facility. Road segments inside each grid cell are firstly obtained, and then constructed as a road network, the assortativity of the road network inside each grid cell is further calculated using Equation 2^{37,38}.

$$GC_AC_i = \frac{1}{\sigma_q^2} \sum_{jk} jk (e_{jk} - q_j q_k) \quad (2)$$

where, GC_AC_i is the value of assortativity coefficient of grid cell i , q_k is the excess distribution and defined as $q_k = \frac{(k+1)p_{k+1}}{\sum_j j p_j}$, p_k is the degree distribution of the network, e_{jk} is the joint probability distribution of a link having degree j on one end and degree k on the other end, and $\sigma_q^2 = \sum_k k^2 q_k - [\sum_k k q_k]^2$.

Similar to the measurement of robustness of a building, the cell tower age is used to measure the robustness of a communication system. Older cell towers are more vulnerable to disruptive events than newly built ones due to its less advanced materials, design, equipped technology, and construction standards²⁰. The OpenCellID dataset, which provides the precise location information of a cell tower, its service range, and the age of the cell tower is adopted to calculate the cell tower age of each grid cell. The area served by each cell tower is modeled as a circle with the location of the cell tower as the center of the circle and the service range as the radius of this circle. This circle is further named as the service circle of the cell tower. Grid cells intersected with service circle of the cell tower are assumed to be served by this cell tower. The cell tower age of each grid cell is calculated by taking the average value of ages of all cell towers served by this grid cell as shown in Equation 3.

$$GC_CAG_i = \frac{\sum_j C_CA_j}{|CA_i|} \text{ for } j \text{ in } CA_i \quad (3)$$

where, GC_CA_i is the cell tower age of grid cell i , C_CA_j is the cell tower age of cell tower j , CA_i is the set of cell towers that serve grid cell i .

Vulnerability is usually considered as the inverse concept of robustness^{29,41–43}. To this end, following Yin and Mostafavi²⁰'s work, the poverty rate in each grid cell is used to measure the robustness in the society system. Poverty rate dataset in block group level provided by the US Census Bureau is adopted. Mean value of poverty rates in block groups intersected with the grid cell is calculated as the education level of the corresponding grid cell as shown in Equation 4.

$$GC_PV_i = \frac{\sum_j BG_PV_j}{|PV_i|} \text{ for } j \text{ in } PV_i \quad (4)$$

where, GC_PV_i is the poverty rate of grid cell i , BG_BR_j is the poverty rate of block group j intersected with grid cell i , and PV_i is the set of block groups which are intersected with grid cell i .

Measurement of Redundancy

Redundancy is defined as the availability of (substitutable) components with similar (even overlapping) functions in the urban system to enhance its adaptive capacity and ability to absorb shocks, give it reserve capacity for problem solving^{25,44,45}. Numbers of healthcare facilities within an accessible distance are adopted to measure the redundancy of facilities. Healthcare facilities provide the most basic functions of this society to ensure the basic life of residents, which are fundamental for life saving if residents are injured. The high-resolution geographic location information of healthcare centers could be obtained from POI data starting with NAICS code of 621, 622, and 623. The serviced grid cells of each hospital are determined as grid cells which are within 30 minutes driving time to the hospital. The threshold of 30-minute driving time is selected because it is a frequently adopted threshold to determine the serviced patients of the hospital^{46–49}. The estimated shortest distance between grid cells is calculated following the work of et al.⁵⁰. The travel time between grid cells is estimated assuming the travel speed of each road segment is its free-flow speed. When one key facility is disrupted within the accessible distance, residents could change to others ensuring their basic life needs. The abundance of healthcare facilities could ensure the availability of substitutable components crucial for preserving life. This redundancy could help the community resist, recover from, and adapt to disruptions better. With travel time information, for each grid cell, the number of available healthcare centers within 30-minutes driving time could be calculated as shown in Equation 5.

$$HG_i = |\{C_j | d(G_i, C_j) \leq 30\}| \quad (5)$$

where, HG_i is the accessible number of healthcare centers of grid cell i , C_j is the healthcare center j , and $d(G_i, C_j)$ is the driving time from grid cell i to healthcare center j .

The number of roads connected with the grid cell is used to measure the redundancy of transportation as shown in Equation 6. The number of roads connected with the grid cell could ensure the travel outside the grid cell to others. When some roads connected with the grid cell are disrupted, alternative roads could be used to ensure the connection between other grid cells. The larger this index is, the larger the redundancy of the transportation network is to ensure basic mobility (e.g., the movement of rescue resources) among different areas. Links and nodes within each grid cell are obtained and the redundancy is calculated using Equation 6.

$$RI_k = \sum_i RS_i \quad (6)$$

where, RI_k is the number of road segments intersected with the boundary of grid cell k , and RS_i is a binary variable which equals 1 if it is intersected with the boundary of k , otherwise, 0.

Electric communications equipment and antennae are mounted on cell towers, which allows the surrounding areas to use wireless communication devices such as cell phones⁵¹. The number of available cell towers is treated to measure the redundancy of the communication system. If more than one cell tower is available to the grid cell, when one of the cell towers is disrupted, others could provide alternatives for residences in this grid cell to maintain

communication with the outside world. This redundancy is important for coordinating rescue and relief operations after a disaster, ensuring that accurate information can be sent and received by victims despite the challenging circumstances. It will also serve to reassure people affected by the disaster that help is on the way and their situation is known to the outside world. Similar to the calculation of cell tower age, the OpenCellID dataset is also used. The available number of cell towers of each grid cell is calculated as shown in Equation 7.

$$GC_CT_i = |\{C_CT_j | C_CT_j \cap GC_i\}| \quad (7)$$

where, GC_CT_i is the available number of cell tower in grid cell i , C_CT_j is the service circle of the cell tower j , and GC_i is grid cell i .

The Social Connectedness Index (SCI), which measures the “extent to which people with low and high socioeconomic status are friends with each other,”²³ is adopted to measure the redundancy of the society. Residents with dissimilar hazard exposure would help each other through social ties⁵². Those with wider social connections could have more choices to seek assistance to lessen impacts of disruption. That is, when some of their social connections are unable to help them (may be caused by their unwillingness, their inability, etc.), they could seek help from other social connections. This redundancy in social ties could help victims better cope with disruptions and recover more quickly from disruptions⁵². Connectedness statistics at the Zip code level publicly available from Social Capital Atlas²³ are adopted to calculate the social connectedness index of each grid cell. Each grid cell’s SCI value is calculated as the mean value of intersected Zip codes’ SCI as shown in Equation 8:

$$GC_SCI_i = \frac{\sum_j ZC_SCI_j}{|Z_i|} \text{ for } j \text{ in } Z_i \quad (8)$$

where, GC_SCI_i is the SCI value of grid cell i , Z_i is a set of Zip code intersected with grid cell, $|Z_i|$ is the number of elements in set Z_i , and ZC_SCI_j is the SCI value of the j^{th} Zip code intersected with grid cell i .

S4 Measurement of Resourcefulness

Resourcefulness is defined as the ability to effectively use available resources, both internal and external, to adapt, overcome, or mitigate the impacts of disturbances^{16,24}. After disturbances, green space could provide the spare capacity for temporary shelters to accommodate large numbers of victims, and space for building reconstruction⁵³, which could help the community cope with, recover from disturbances better. The total available number of beds for each grid cell is calculated in a manner similar to that of the calculation of available number of healthcare centers. National Land Cover Database (NLCD) is adopted to calculate the area of green space of each grid cell. The area of land use type 71 (grassland/herbaceous) in each grid cell is calculated as its green space area.

$$GS_BC_i = \sum_j G_BC_j \text{ for } j \text{ in } GS_j \quad (9)$$

where, GS_BC_i is the green space area of grid cell i , G_BC_j is the intersected area of NLCD pixel in type 71 cell j with grid cell i , and GS_j is the set of NLCD pixels intersected with grid cell i .

Road density is used to measure the resourcefulness of the transportation system. A higher road density can improve access to important locations, such as evacuation facilities and hospitals⁵⁴. This is particularly vital during emergencies when rapid response and evacuation are necessary. Thus, in the face of disturbances, the denser road network would facilitate evacuation of victims and would ensure rescue resources reach affected communities quickly^{55,56}. Road segments inside each grid cell were obtained to calculate the robustness of the transportation system. The total length of road segments inside each grid cell is then calculated, and it is further divided by the area of grid cell to obtain the value of road density.

Internet speed measures the resourcefulness of a communication system. When faced with disruptive events, faster internet speed ensures that communities have access to real-time, reliable information which are crucial in helping them prepare for, respond to, and recover from disruptive events, as well as ensure effective coordination among emergency services. Internet speed dataset which is publicly accessible from Ookla in the resolution of zoom level 16 Web

Mercator Tiles (in the shape of pixel) is used. For each grid cell, its internet speed is calculated as the average internet speed of all pixels that intersect with it as shown in Equation 10.

$$GC_IS_i = \frac{\sum_j P_IS_j}{|IS_i|} \text{ for } j \text{ in } IS_i \quad (10)$$

where, GC_IS_i is the internet speed of grid cell i , P_IS_j is the internet speed of pixel j , and IS_i is the set of pixels intersected with grid cell i .

Resourcefulness could be interpreted as both the available external material resources and the residence's internal capacity to identify problems and apply available resources²⁴ to adapt, overcome, or mitigate the impacts. Education level is adopted to measure the resourcefulness of society from the second aspect (the residence's ability to apply available resources). Higher education level usually results in better comprehension of data and information related to potential hazards and their disturbances and more effective emergency response¹⁶. Education could also increase a person's ability to access, understand, and utilize information, and improve critical thinking and problem-solving abilities¹⁶, which are all critical in making effective strategies in the face of disturbances. The bachelor's degree rate dataset at the census block level provided by US Census Bureau is adopted. Mean value of bachelor rates in block groups intersected with the grid cell is calculated as the education level of the corresponding grid cell as shown in Equation 11.

$$GC_EL_i = \frac{\sum_j BG_BR_j}{|BR_i|} \text{ for } j \text{ in } BR_i \quad (11)$$

where, GC_EL_i is the education level of grid cell i , BG_BR_j is the bachelor rate of block group j intersected with grid cell i , and BR_i is the set of block groups which are intersected with grid cell i .

Node representation learning

An autoencoder model, stacked denoising autoencoders (SDAE) developed by Vincent et al.⁵⁷, are deployed to capture complex and nonlinear interactions among individual community resilience-related features by encoding these features into latent representations. In SDAE, the autoencoder is first pre-trained in the sub-autoencoder level. Each sub-autoencoder is a denoising autoencoder which is a neural network that receives a corrupted data as input and is trained to reconstruct the original uncorrupted data as output, which is defined as⁵⁷:

$$\begin{aligned} \tilde{x} &= Dropout(x) \\ h &= f_1(W_1\tilde{x} + b_1) \\ \tilde{h} &= Dropout(h) \\ y &= f_2(W_2\tilde{h} + b_2) \end{aligned} \quad (12)$$

where x is the original uncorrupted data, \tilde{x} is the actual input data of encoder layer obtained after dropout, f_1 and f_2 are activation functions for the encoding and decoding layer, respectively, and $\{W_1, b_1, W_2, b_2\}$ are trainable model parameters. As we aim to reconstruct the uncorrupted data, the loss function is designed as $\|x - y\|_2^2$. The rectified linear unit (ReLU) is adopted as the activation function for each sub-autoencoder, except for f_1 of the last sub-autoencoder to make the final node embeddings preserve full information⁵⁷. The embedding obtained through the encoder layer is used as the input of next sub-autoencoder to train it.

After greedy layer-wise pre-train, the encoder layer in each sub-autoencoder is concatenated followed by all decoder layers in reverse lay-wise training order⁵⁷. A deep autoencoder is thus developed and then fine-tuned to minimize reconstruction loss⁵⁷. The resilience-feature matrix is passed through the encoder layers of this fine-tuned deep autoencoder (f_e) to obtain the encoded representations (E).

Clustering

Inspired from Xie et al.⁵⁸, 's work, a self-training strategy is employed to jointly optimize the assignment of cluster labels and learn features conducive for clustering. Xie et al.⁵⁸, proposed to obtain the final clustering result through alternating between two steps until a convergence criterion is reached. First, a soft assignment between E and the cluster centroids are calculated. Sencod, a high confidence assignment is learned using an auxiliary target distribution. It is

further used to update f_e for more cluster-friendly embeddings and refine cluster centroids.

The standard k -means clustering is used once on \mathbf{E} to obtain initial cluster centroids u_j . Following the work of Maaten and Hinton⁵⁹, the S t -distribution is used as a kernel to measure the similarity between embedding z_i and u_j :

$$q_{ij} = \frac{(1 + \|z_i - u_j\|^2/\alpha)^{-\frac{\alpha+1}{2}}}{\sum_{j'} (1 + \|z_i - u_{j'}\|^2/\alpha)^{-\frac{\alpha+1}{2}}} \quad (13)$$

where z_i is the i -th sample of \mathbf{E} , q_{ij} is the probability of assigning sample i to cluster center j , and α is the degree of freedom of the t -distribution and it is set to be 1 following the work of Xie et al.⁵⁸.

Following Xie et al.⁵⁸, the auxiliary target distribution (P) is defined by first raising q_i to the second power and then normalizing by frequency per cluster:

$$p_{ij} = \frac{q_{ij}^2/f_j}{\sum_{j'} q_{ij'}^2/f_{j'}} \quad (14)$$

where $f_j = \sum_i q_{ij}$ are soft cluster frequencies. The soft assignment (Q) is trained to match the auxiliary target distribution (P) by minimizing the KL divergence loss between the soft assignment (q_i) and the auxiliary target distribution (p_i) as follows⁵⁸:

$$L = KL(P||Q) = \sum_i \sum_j p_{ij} \frac{p_{ij}}{q_{ij}} \quad (15)$$

The most likely cluster k that instance i belongs (s_i) to is.

$$s_i = \underset{k}{\operatorname{argmax}}(q_{ik}) \quad (16)$$

Community resilience level determination

Grid cells in the same group are assumed to have the same community-resilience level due to the clustering module having clustered grid cells with similar community resilience into the same group. The clustering module also ensures that grid cells in different clusters are different from each other as much as possible.

Inspired from the work of Morichetta et al.⁶⁰ work, an explainable classification model is implemented to interpret the clustering results. We do this by training an explainable classification model on the clustering results obtained in the second layer of the model, i.e., using the clustering results as the labels of the classification model then interpreting the cluster assignment results modeled by the explainable classifier.

The random forests classifier⁶¹ was selected as the explainable classification model considering its interpretability and performance. Random forests classifier is implemented using Scikit-learn⁶² by taking resilience-related feature matrix as input and setting clustering results as labels, and details of random forests classifier is described in the work of Breiman⁶¹.

After obtaining feature importance of individual resilience-related feature to the final clustering results, the community-resilience level is determined as follows:

1. Following Siam et al.⁶³, Xu et al.⁶⁴, and Yin and Mostafavi²⁰'s work community resilience-related features are normalized to reduce the impact of the difference of unit using Min-Max scaler:

$$x' = \frac{x - x_{min}}{x_{max} - x_{min}} \quad (17)$$

where x' is the scaled value which is in the range of $[0,1]$.

2. Following the work of Yin and Mostafavi²⁰ work, calculate each community resilience-related feature's mean values for each cluster:

$$\overline{R_{iku}} = \frac{\sum_{l=1}^n R_{iku-l}}{n} \quad (18)$$

where $\overline{R_{iku}}$ is the average value for feature i in cluster k in MSA u , and R_{iku-l} is the l -th value of feature i in cluster k in MSA u .

- The aggregated community resilience value of each cluster is calculated by weighted sum of each resilience-related feature by taking feature importance as the weight:

$$AR_{ku} = \sum_i IM_i * \overline{R_{tku}} \quad (19)$$

where IM_i is the importance of feature i to the clustering result, and AR_{ku} is the aggregated resilience value of cluster k in MSA u .

- Finally, calculate the flood risk level value RL_{ku} by ranking the value of AR_{ku} in an ascending way:

$$RL_{ku} = Sorted(AR_{ku}) \quad (20)$$

Parameters setting

We set the searching space for each hyperparameter in *Resili-Net* and use grid search to select the optimal set of hyperparameters. The network dimension of f_e is set as $d_{in} - 500 - 500 - 2000 - d_e$, where d is the input dimension, and d_e is the embedding dimension which is grid searched from [10, 12, 24, 36]. The pre-train and fine-tune epochs are set at 200. The dropout rate is set at 0.2. The batch size is set at 256. The learning rate is set at 0.1. The clustering number is grid searched from [4, 5, 6, 7].

The performance of the classifier is evaluated by precision, recall, and F1-score in macro-, micro, and the value of AUC. Definitions of these evaluations can be referenced in the work of Ho et al.⁶⁵. The random forest classifier is capable of modeling, almost entirely, the clustering results, with AUC, F1-score, recall, precision values all close to 1 for all four clustering (Fig. 8). This demonstrates that the classifier is able to represent the obtained cluster assignments as classification classes, and can be automatically used to interpret the allocation of instances to each cluster.

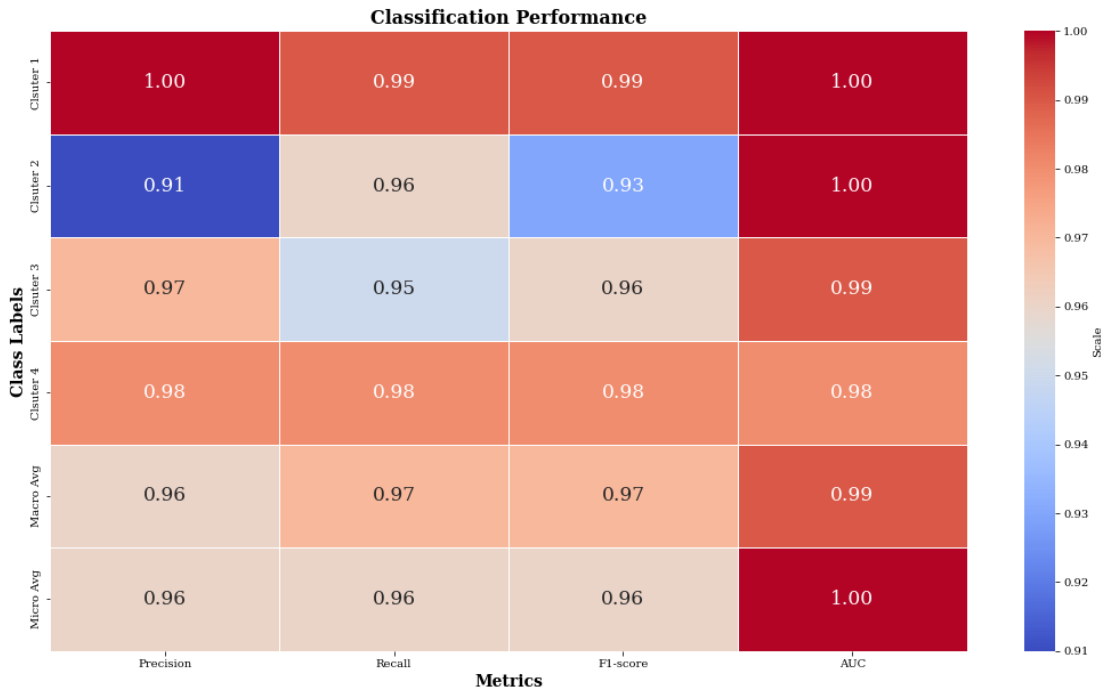


Fig. 8 | Performances of random forest classifier results with cluster results as labels for Greater Houston. Other three MSAs are in Figs. S8–10.

Data Availability

The dataset used in this paper are publicly accessible and cited in this paper.

Code Availability

The code that supports the findings of this study is available from the corresponding author upon request.

Acknowledgements

This work was supported by National Science Foundation under CRISP 2.0 Type 2 No. 1832662 grant. Any opinions, findings, conclusions, or recommendations expressed in this research are those of the authors and do not necessarily reflect the view of the funding agencies.

Author contributions

Kai Yin: Conceptualization, Methodology, Software, Formal analysis, Investigation; Writing, original draft; writing, review, and editing; Visualization. **Ali Mostafavi:** Conceptualization; Methodology; Writing, Reviewing and Editing; Supervision; Funding acquisition.

Competing interests

The authors declare no competing interests.

Additional information

Supplementary material associated with this article can be found in the attached document.

References

1. Rus, K., Kilar, V. & Koren, D. Resilience assessment of complex urban systems to natural disasters : A new literature review. *International Journal of Disaster Risk Reduction* **31**, 311–330 (2018).
2. Liu, Z., Liu, C. & Mostafavi, A. Beyond Residence : A Mobility-based Approach for Improved Evaluation of Human Exposure to Environmental Hazards. (2023).
3. Liu, Z. & Mostafavi, A. Collision of Environmental Injustice and Sea Level Rise : Assessment of Risk Inequality in Flood-induced Pollutant Dispersion from Toxic Sites in Texas Abstract : (2023).
4. Debortoli, N. S., Sayles, J. S., Clark, D. G. & Ford, J. D. A systems network approach for climate change vulnerability assessment A systems network approach for climate change vulnerability assessment. *Environmental Research Letters* (2018).
5. Thakur, S., Negi, V. S., Pathak, R., Dhyani, R. & Durgapal, K. Forest Ecology and Management Indicator based integrated vulnerability assessment of community forests in Indian west Himalaya. *Forest Ecology and Management* **457**, 117674 (2020).
6. Sowman, M. & Raemaekers, S. Socio-ecological vulnerability assessment in coastal communities in the BCLME region. *Journal of Marine Systems* **188**, 160–171 (2018).
7. Esmalian, A. *et al.* Operationalizing resilience practices in transportation infrastructure planning and project development. *Transportation Research Part D* **104**, 103214 (2022).
8. Lee, C. C. *et al.* Quantitative measures for integrating resilience into transportation planning practice: Study in Texas. *Transportation Research Part D: Transport and Environment* **113**, (2022).
9. Rajput, A. A. & Mostafavi, A. Latent sub - structural resilience mechanisms in temporal human mobility networks during urban flooding. *Scientific Reports* 1–14 (2023) doi:10.1038/s41598-023-37965-6.
10. Yin, K., Wu, J., Wang, W., Lee, D. & Wei, Y. An integrated resilience assessment model of urban transportation network : A case study of 40 cities in China. *Transportation Research Part A* **173**, 103687 (2023).
11. Bhusal, N. & Member, S. Power System Resilience : Current Practices , Challenges , and Future Directions. *IEEE Access* **8**, 18064–18086 (2020).
12. Wang, Y. *et al.* Research on Resilience of Power Systems Under Natural Disasters — A Review. *IEEE Transactions on Power Systems* **31**, 1604–1613 (2016).
13. Tan, B. Sen, Wu, Y., Xie, P. & Guerrero, J. M. New Challenges in the Design of Microgrid Systems. (2020) doi:10.1109/MELE.2020.3026496.
14. Saja, A. M. A., Teo, M., Goonetilleke, A. & Ziyath, A. M. An inclusive and adaptive framework for measuring social resilience to disasters. *International Journal of Disaster Risk Reduction* **28**, 862–873 (2018).
15. Fan, C., Xu, J., Natarajan, B. Y. & Mostafavi, A. Interpretable machine learning learns complex interactions of urban features to understand socio-economic inequality. *Computer-Aided Civil and Infrastructure Engineering* 1–17 (2023) doi:10.1111/mice.12972.
16. Huang, G., Li, D., Zhu, X. & Zhu, J. Influencing factors and their influencing mechanisms on urban resilience in China. *Sustainable Cities and Society* **74**, 103210 (2021).
17. Parizi, S. M., Taleai, M. & Sharifi, A. Integrated methods to determine urban physical resilience characteristics and their interactions. *Natural Hazards* **109**, 725–754 (2021).
18. Kutty, A. A., Wakjira, T. G., Kucukvar, M., Abdella, G. M. & Onat, N. C. Urban resilience and livability performance of European smart cities: A novel machine learning approach. *Journal of Cleaner Production* **378**, 134203 (2022).
19. NIAC. Critical Infrastructure Resilience Final Report and Recommendations. (2009).
20. Yin, K. & Mostafavi, A. Unsupervised Graph Deep Learning Reveals Emergent Flood Risk Profile of Urban Areas. *arXiv preprint arXiv:2309.14610* (2023).
21. CDC(Centers for Disease Control and Prevention). CDC/ATSDR Social Vulnerability Index 2020. 15–16 <https://www.atsdr.cdc.gov/placeandhealth/svi/index.html> (2023).

22. US Army(US Army Corps of Engineers Hydrologic Engineering Center). NSI Technical Documentation. <https://www.hec.usace.army.mil/confluence/nsi/technicalreferences/latest/technical-documentation> (2022).
23. Chetty, R. *et al.* Social capital I: measurement and associations with economic mobility. *Nature* **608**, 108–121 (2022).
24. Bruneau, M. *et al.* A Framework to Quantitatively Assess and Enhance the Seismic Resilience of Communities. *Earthquake Spectra* **19**, 733–752 (2003).
25. Sharifi, A. & Yamagata, Y. Principles and criteria for assessing urban energy resilience: A literature review. *Renewable and Sustainable Energy Reviews* **60**, 1654–1677 (2016).
26. Tong, P. Characteristics , dimensions and methods of current assessment for urban resilience to climate-related disasters : A systematic review of the literature. *International Journal of Disaster Risk Reduction* **60**, 102276 (2021).
27. Leobons, C. M. *et al.* A Proposal of Assessing Urban Transportation Systems Resilience : A Proposal of Indicators Indicators. *Transportation Research Procedia* **37**, 322–329 (2019).
28. TIERNEY, K. & MICHEL, B. A Key to Disaster Loss Reduction. *TR NEWS* (2007).
29. Gu, Y., Fu, X., Liu, Z., Xu, X. & Chen, A. Performance of transportation network under perturbations: Reliability, vulnerability, and resilience. *Transportation Research Part E: Logistics and Transportation Review* **133**, 1–16 (2020).
30. Fernandez, P., Mourato, S., Moreira, M. & Pereira, L. A new approach for computing a flood vulnerability index using cluster analysis. *Physics and Chemistry of the Earth* **94**, 47–55 (2016).
31. M. Neubert, T. Naumann, J. H. and J. N. The Geographic Information System-based flood damage simulation model HOWAD. *Flood Risk Management* (2016) doi:10.1111/jfr3.12109.
32. Simonovic, S. P. *et al.* *Floods : Mapping Vulnerability in the Upper Thames Watershed under a Changing Climate.* (2007).
33. Wang, W. *et al.* Network approach reveals the spatiotemporal influence of traffic on air pollution under COVID-19. (2022) doi:10.1063/5.0087844.
34. Qi, H., Li, X., Yin, K. & Xiangnan Song, X. F. Sustainable development-oriented campus bike- sharing site evaluation model : A case study of Henan Polytechnic University Code , Data and Media Associated with this Article. *arXiv* 7–10 (2023).
35. Yin, K., Li, X., Chen, Q. & Lu, J. Examining the Reasons for the Low Market Share of Road Passenger Transport Based Express Using Structural Equation Modeling. in 459–471 (2018).
36. Rajput, A. A., Li, Q., Gao, X. & Mostafavi, A. Revealing Critical Characteristics of Mobility Patterns in New York City During the Onset of COVID-19 Pandemic. **7**, 1–12 (2022).
37. Newman, M. E. J. Assortative Mixing in Networks. 1–4 (2002) doi:10.1103/PhysRevLett.89.208701.
38. Newman, M. E. J. Mixing patterns in networks. *Physical Review E: Statistical, Nonlinear, and Soft Matter Physics* (2003).
39. Derrible, S. & Kennedy, C. The complexity and robustness of metro networks. *Physica A* **389**, 3678–3691 (2010).
40. Dong, S. *et al.* Measuring the Topological Robustness of Transportation Networks to Disaster-Induced Failures : A Percolation Approach. **26**, 1–17 (2020).
41. de Oliveira, E. L., Portugal, L. da S. & Porto Junior, W. Indicators of reliability and vulnerability: Similarities and differences in ranking links of a complex road system. *Transportation Research Part A: Policy and Practice* **88**, 195–208 (2016).
42. Reggiani, A., Nijkamp, P. & Lanzi, D. Transport resilience and vulnerability: The role of connectivity. *Transportation Research Part A: Policy and Practice* **81**, 4–15 (2015).
43. Mattsson, L. G. & Jenelius, E. Vulnerability and resilience of transport systems - A

- discussion of recent research. *Transportation Research Part A: Policy and Practice* **81**, 16–34 (2015).
44. Sharifi, A. & Yamagata, Y. Major Principles and Criteria for Development of an Urban Resilience Assessment Index. (2014).
 45. Tyler, S. & Moench, M. A framework for urban climate resilience. **5529**, (2012).
 46. Shen, Y. C. & Hsia, R. Y. Differential benefits of cardiac care regionalization based on driving time to percutaneous coronary intervention. *Academic Emergency Medicine* **28**, 519–529 (2021).
 47. Rayburn, W. F., Richards, M. E. & Elwell, E. C. Drive times to hospitals with perinatal care in the United States. *Obstetrics and Gynecology* **119**, 611–616 (2012).
 48. Chang, J. *et al.* Driving Time to the Nearest Percutaneous Coronary Intervention-Capable Hospital and the Risk of Case Fatality in Patients with Acute Myocardial Infarction in Beijing. *International Journal of Environmental Research and Public Health* **20**, (2023).
 49. Koeze, E., Patel, J. K. & Singhvi, A. Where Americans Live Far From the Emergency Room. *The New York Times* 1–11 (2020).
 50. Fan, C., Jiang, X., Lee, R. & Mostafavi, A. Equality of access and resilience in urban population-facility networks. *npj Urban Sustainability* **2**, 1–12 (2022).
 51. Company, M. N. L. S. What Is a Cell Tower and How Does a Cell Tower Work ? 1–13 <https://millmanland.com/company-news/what-is-a-cell-tower-and-how-does-a-cell-tower-work/> (2023).
 52. Liu, C. F. & Mostafavi, A. Revealing hazard - exposure heterophily as a latent characteristic of community resilience in social - spatial networks. *Scientific Reports* 1–8 (2023) doi:10.1038/s41598-023-31702-9.
 53. Shrestha, S. R., Sliuzas, R. & Ku, M. Open spaces and risk perception in post-earthquake Kathmandu city. **93**, 81–91 (2018).
 54. Bozza, A., Asprone, D. & Manfredi, G. Developing an integrated framework to quantify resilience of urban systems against disasters. *Natural Hazards* **78**, 1729–1748 (2015).
 55. Sakakibara, H., Kajitani, Y. & Okada, N. Road Network Robustness for Avoiding Functional Isolation in Disasters. 560–567 (2004) doi:10.1061/(ASCE)0733-947X(2004)130.
 56. Kotzee, I. & Reyers, B. Piloting a social-ecological index for measuring flood resilience : A composite index approach. *Ecological Indicators* **60**, 45–53 (2016).
 57. Vincent, P., Larochelle, H., Lajoie, I., Bengio, Y. & Manzagol, P. A. Stacked denoising autoencoders: Learning Useful Representations in a Deep Network with a Local Denoising Criterion. *Journal of Machine Learning Research* **11**, 3371–3408 (2010).
 58. Xie, J., Girshick, R. & Farhadi, A. Unsupervised deep embedding for clustering analysis. *33rd International Conference on Machine Learning, ICML 2016* **1**, 740–749 (2016).
 59. Maaten, L. van der & Hinton, G. Visualizing Data using t-SNE. *Journal of Machine Learning Research* **219**, 187–202 (2008).
 60. Morichetta, A., Casas, P. & Mellia, M. Explain-IT: Towards explainable AI for unsupervised network traffic analysis. *Big-DAMA 2019 - Proceedings of the 3rd ACM CoNEXT Workshop on Big Data, Machine Learning and Artificial Intelligence for Data Communication Networks, Part of CoNEXT 2019* 22–28 (2019) doi:10.1145/3359992.3366639.
 61. BREIMAN, L. RANDOM FORESTS. in *International Journal of Advanced Computer Science and Applications* vol. 7 1–33 (2001).
 62. Pedregosa, F., Varoquaux, G., Gramfort, A., Michel, V. & Thirion, B. Scikit-learn: Machine Learning in Python Fabian. *Journal of Machine Learning Research* **127**, 2825–2830 (2019).
 63. Siam, Z. S. *et al.* National-scale flood risk assessment using GIS and remote sensing-based hybridized deep neural network and fuzzy analytic hierarchy process models: a

- case of Bangladesh. *Geocarto International* **0**, 1–30 (2022).
64. Xu, H., Ma, C., Lian, J., Xu, K. & Chaima, E. Urban flooding risk assessment based on an integrated k-means cluster algorithm and improved entropy weight method in the region of Haikou, China. *Journal of Hydrology* **563**, 975–986 (2018).
 65. Ho, Y., Hsiao, T. & Chen, A. Y. Emission Analysis of Electric Motorcycles and Assessment of Emission Reduction With Fleet Electrification. *IEEE Transactions on Intelligent Transportation Systems* **PP**, 1–10 (2023).